Switching Chirality of Hybrid Left−Right Crystalline Helicoids Built of Achiral Polymer Chains: When Right to Left Becomes Left to Right

ARTICLE *in* MACROMOLECULES · NOVEMBER 2014

Impact Factor: 5.8 · DOI: 10.1021/ma501733n

Macromolecules

Article

pubs.acs.org/Macromolecules

Switching Chirality of Hybrid Left−Right Crystalline Helicoids Built of Achiral Polymer Chains: When Right to Left Becomes Left to Right

Martin Rosenthal,*[,†] Manfred Burghammer,[‡,§] Georg Bar,[∥] Edward T. Samulski,[⊥] and Dimitri A. Ivanov*[,†,#]

[†]Institut de Sciences des Matériaux de Mulhouse, CNRS UMR 7361, 15 rue Jean Starcky, 68057 Mulhouse, France

[‡]European Synchrotron Radiation Facility, 6 rue Jules Horowitz, 38043 Grenoble, France

[§]Department of Analytical Chemistry, Ghent University, Krijgslaan 281, S12, B-9000 Ghent, Belgium

[∥]Analytical Technology Center, Analytical Technologies, Dow Olefinverbund GmbH, 06258 Schkopau, Germany

[⊥]Department of Chemistry, University of North Carolina, Chapel Hill, North Carolina 27599-3290, United States

[#]Faculty of Fundamental Physical and Chemical Engineering, Moscow State University, GSP-1, Leninskie Gory, 119991 Moscow, Russian Federation

ABSTRACT: It is widely accepted that achiral polymers crystallize in lamella helicoids of both handedness, whereas chiral polymers are known to form helicoids of only one handedness. By employing nanofocus X-ray diffraction, we show that the situation is more complex and that the lamella helicoids of achiral polymers can be in fact hybrid, i.e., containing a left- and a right-handed part. Moreover, our data demonstrate that the poly(trimethylene terephthalate) lamellae invert chirality at a certain crystallization temperature. The chirality correlates with the growth axis polarity (i.e., a versus $-a$) and handedness of the lamellar helicoid (L versus R) and can be conveniently expressed in terms of the chirality parameter pairs. In addition, the overall chain tilt does not affect the rate and sense of twisting, calling into question the premise of the Keith and Padden model. Instead, the inclination of the terminal segment of the crystalline stem protruding the lamellar surface is proposed to be the key factor controlling the surface stresses.

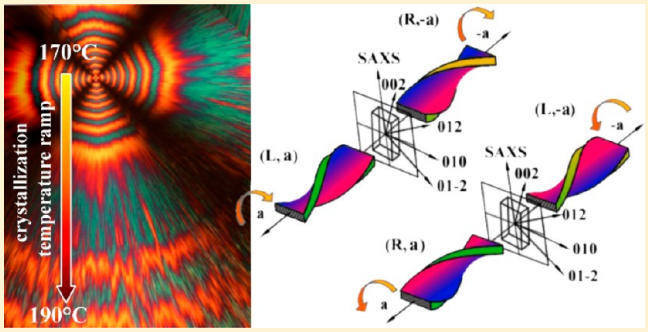

INTRODUCTION

Many crystallizable polymers exhibit a fine substructure within their spherulitic morphology consisting of regularly spaced concentric rings visible in crossed polars, i.e., the so-called banded spherulites. In the past, numerous works addressed the details of the origins of the banded spherulite structure where, in most cases (Keith and Padden[1] and Keller[2]), it was assigned to synchronously twisting lamella crystals growing from the spherulite center. Only in a relatively small number of cases the observed banding resulted from periodic diffusion-induced rhythmic growth.[3]

As far as synchronously twisting lamellar crystals are concerned, according to Keith and Padden,[4] the lamellar twist stems from differences in the congestion of the chain folds on the lamellar basal planes. This is generated in turn by the chain tilt which adds a chiral element to the lamella structure. The Keith and Padden model (KP model) was initially designed specifically for polyethylene (PE) where it correctly describes the correlation between the tilt of the chain stem with respect to the normal to the lamella basal plane and the twisting direction of the crystal. However, being largely empirical in nature, the model does not account for the exact mechanism via which the inclination of the stem generates differential stresses in the top and bottom parts of the lamella.

To explain the morphogenesis of the polymer spherulites, Keith and Padden[5] suggested that a gradient of the driving force of crystallization caused by the diffusion field at the growth front of the polymer crystal results in the possibility of a morphological instability; this causes the crystal branching. A model discussed by Toda[6] assumes that the branching instability of the growth front and the reorientation of the branches are driven by the torsional stress and result in a helical twist of the lamellar crystals.

However, the correlation between the chirality of the structure at different scales is still a matter of debate. It is often assumed that achiral polymers can form lamellar helicoids of both handedness, whereas chiral polymers are documented to form only one type of helicoid, i.e., either right- or left-handed. The reasons for the choice of the handedness of the lamellar helicoids are not yet fully understood and are re-examined herein.

Received: August 22, 2014
Revised: October 7, 2014
Published: November 19, 2014

   dx.doi.org/10.1021/ma501733n | *Macromolecules* 2014, 47, 8295−8304

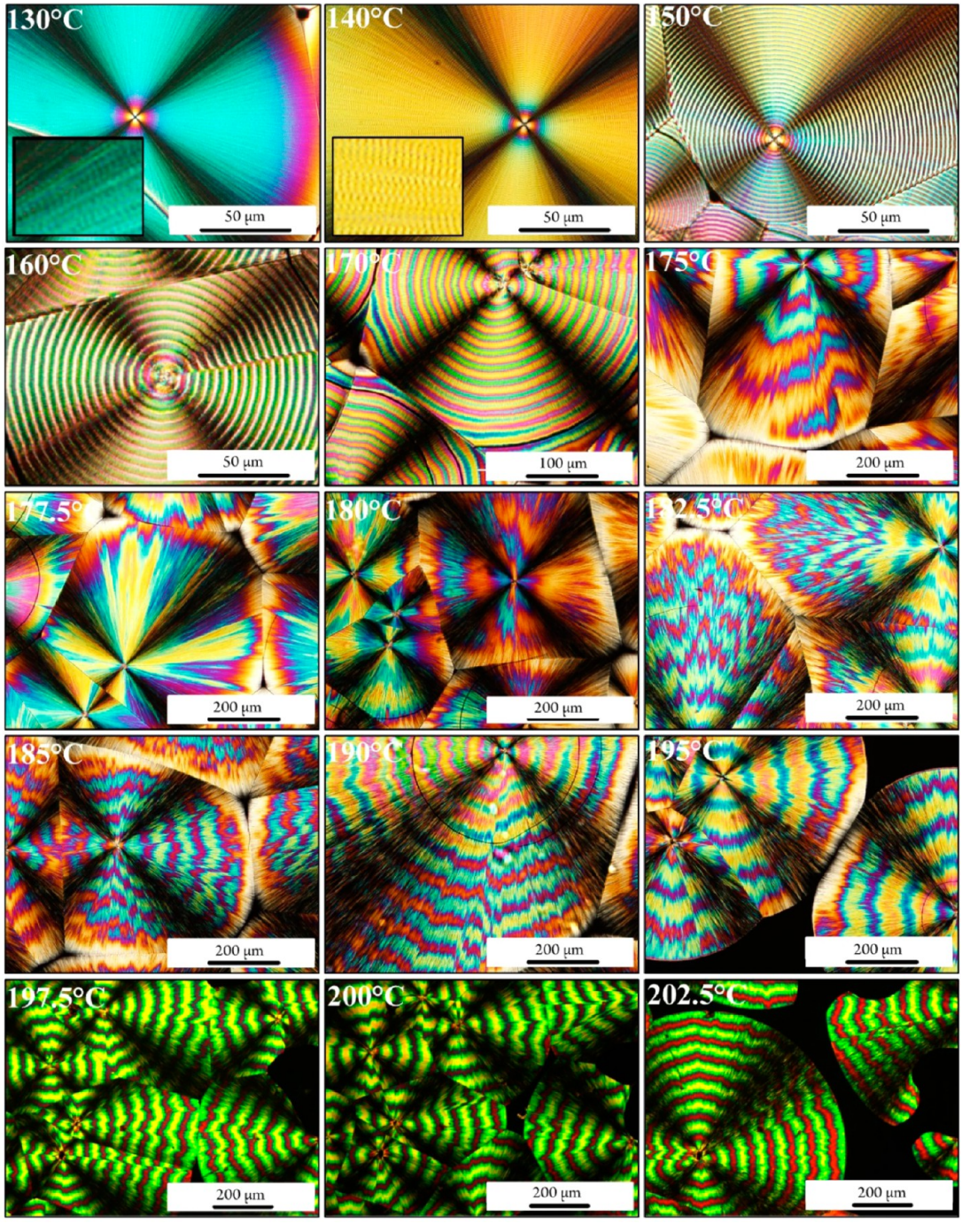

Figure 1. Polarized optical micrographs of PTT spherulites grown from the melt at various temperatures in the range from 130 to 202.5 °C. The images are used to evaluate the dependence of the band spacing on the crystallization temperature.

Synchrotron micro- and nanobeam X-ray diffraction was recently demonstrated to be a powerful technique for morphological studies of polymeric materials. In the case of polymer spherulites exhibiting bands, it enabled the exploration of such local-scale morphological features as crystal growth direction, crystal orientation, and degree of order.[7,8] Therefore, the experimental verification of the discussed models has now become possible, as was reported in a recent work on banding in the spherulites of bulk PE.[9] It was shown for the first time that the direction of the stem tilt correlates indeed with the direction of lamella twist, as predicted in the KP model. The KP model and its relevance to banding in poly(trimethylene terephthalate), PTT, are discussed in detail in our previous publication that uses the microfocus X-ray diffraction methodology.[10]

In the present work, we employ the microfocus X-ray diffraction for an in-depth analysis of the banded spherulite microstructure with a goal of identifying the twisted lamella growth mechanisms. In particular, we attempt to verify the correlations between the chirality of the lamellar helicoids and the chain tilt direction, a key parameter of the KP model. In the course of the discussion of our findings, it will be shown that this model cannot account for certain features of the PTT lamellar twisting behavior, in particular, instances where the

dx.doi.org/10.1021/ma501733n | *Macromolecules* 2014, 47, 8295−8304

chirality of the lamellar twist can invert with crystallization temperature. In an attempt to explain our observations, we will correlate the complex temperature dependence of the banding behavior with the lamellar thickness.

EXPERIMENTAL SECTION

Poly(trimethylene terephthalate) (PTT) with weight-average molecular mass M_w = 35 200 g/mol and polydispersity M_w/M_n = 2 was received from Shell Chemicals (grade Corterra CP 509200). The samples were prepared between cover glass slides resulting in approximately 20 μm thick films; they were crystallized isothermally from the melt in the temperature range from 130 to 205 °C. A short dwelling time in the melt, specifically 2 min at 260 °C, was used to erase the structural memory before the isothermal crystallization. Upon cooling to room temperature, free-standing films were obtained by immersing the films in 1% aqueous solution of HF for 24 h. In the experiments, the PTT banding behavior was always uniform across the entire sample.

Nanobeam X-ray scattering experiments in transmission have been carried out using the microbeam facility at the ID13 beamline of the European Synchrotron Radiation Facility (ESRF) (Grenoble, France). The submicron X-ray beam was focused down to a spot size of 0.5 μm along both axes using crossed-Fresnel optics. Photons with energy of 12 keV were used in the experiments. 2D diffraction data were collected using a FreLon CCD detector. Several diffraction peaks of corundum were used to calibrate the norm of the scattering vector **s** where $|s| = 2\sin(\theta)/\lambda$. After approximate localization of the region of interest with an on-axis optical microscope, the refinement of the beam position with respect to the PTT spherulite center was performed using the azimuthal positions of selected diffraction peaks on the 2D diffractograms. For interpretation of the diffractograms, the triclinic unit cell of PTT with the following parameters was assumed, where a = 4.60, b = 6.22, c = 18.36, α = 97.8°, β = 90.8°, and γ = 111.3°.[11] To perform lateral scans, a hexapod was used, allowing translation with steps of 1 μm while ensuring precision of 50 nm. The data reduction and analysis including geometrical and background correction, visualization, and integration of the 2D diffractograms were performed employing home-built routines designed in Igor Pro software (Wavemetrics Ltd.).

Small-angle X-ray scattering experiments were conducted at the BM26 beamline of the ESRF (Grenoble) and the A2 beamline of HASYLAB/DESY (Hamburg). All the measurements were conducted in transmission. The PTT films were wrapped between aluminum foils to provide a good temperature contact with the furnace. The bulk samples were melted at 260 °C for 2 min and then quenched to the desired crystallization temperature. The samples were allowed to crystallize for 10−40 min, depending on the crystallization temperature (T_c) and measured at T_c. For calibration, eight orders of rat-tail collagen diffraction were used. The calculation of the 1D-correlation (CF) and interface distribution (IDF) functions was performed using home-built routines; the calculations closely followed the approach described in detail in refs 12 and 13.

RESULTS AND DISCUSSION

Variation of the Band Spacing with Crystallization Temperature. A set of polarized optical micrographs of PTT films crystallized at temperatures ranging from 130 up to 202.5 °C are displayed in Figure 1. All of the shown morphologies clearly exhibit spherulite banding. The colors in the images measured in crossed-polarized light originate from the fact that PTT has a strong birefringence, as reported by Yun and coauthors.[14]

Importantly, Figure 1 reveals a strong variation of the spherulite band spacing with crystallization temperature. Thus, the bands are very tight at 130 °C, where the spacing is on the order of 1 μm (cf. inset in the figure), while it increases up to several hundred microns at 175 °C. At about 180 °C, the bandwidth diverges and exceeds the spherulite diameter and therefore cannot be quantified. At even higher temperatures the banding reappears.

The banded spherulite morphologies also differ in terms of their lateral coherence. At low crystallization temperatures ranging from 130 up to 170 °C, the bands form smooth concentric rings, whereas at higher crystallization temperatures they become jagged. Thus, the lateral correlation of the lamellar stacks weakens with the increase of the band spacing. Starting from approximately 180 °C, the decrease of the band spacing is accompanied by some improvement of the lateral correlation.

The variation of the band spacing as a function of crystallization temperature obtained from the optical microscopy is summarized in Figure 2. The graph reveals a singularity

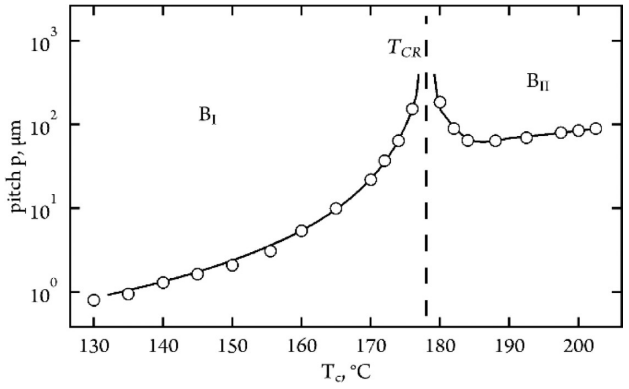

Figure 2. Band spacing for the isothermally crystallized spherulites of PTT as a function of crystallization temperature. In the low-temperature region B_I the band spacing strongly increases, becoming virtually infinite at a "critical" temperature T_{CR}. By contrast, in the high-temperature region (B_{II}) the band spacing first decreases and then slightly increases again.

point at approximately 179 °C, at which the band spacing virtually diverges. Above this point, it starts to decrease up to ca. 187 °C and then resumes a slight increases with temperature. It is noteworthy that at crystallization temperatures below 130 °C the spherulite banding cannot be observed with optical microscopy because of insufficient resolution.

The initial increasing segment of the temperature-dependent band spacing, i.e., the curve before temperature B_I, can be well approximated with the power law function:

$$p \cong \left(\frac{T_{CR} - T}{T_{CR}}\right)^n \quad (1)$$

In eq 1, P and T_{CR} correspond to the band spacing and the "critical" temperature, respectively. The parameters found from the best fit are T_{CR} = 178.7 °C and n = −2 ± 0.09. It is noteworthy that there were already attempts to describe the temperature dependence of the band spacing in PTT using the same type of function. Chuang et al.[15] found a critical exponent of 0.5, which, in his view, could be compared to the well-known critical exponent of the order parameter in the mean-field theory of the equilibrium phase transitions.[16,17] However, in our case it is clear that, overall, the temperature dependence of the band spacing cannot be fitted to a single power-law expression. Moreover, those authors observed that the banded-nonbanded (BNB) transition for PTT occurs at 195 °C on the low temperature side and at ca. 215 °C on the high temperature side.[18] In contrast, we have not observed neither low- nor high-

dx.doi.org/10.1021/ma501733n | Macromolecules 2014, 47, 8295−8304

temperature BNB transitions. Importantly, the results of Chuang and Hong also strongly differ from other reports on PTT. For example, Wu and Woo[19] report that the BNB transitions of PTT occur at 150 and 215 °C, while in the work of Wang et al.[20] the temperature window of the banded morphology is restricted to the range 135 and 165 °C.

In this context, it is worth mentioning an alternative model accounting for the variation of the band spacing with crystallization temperature. The model describes banding as a sequence of successive isochiral screw dislocations activated by thermal fluctuations, as initially proposed by Basset and Hodge[21] and further developed by Toda.[6,22−24] The successive isochiral screw dislocations lead to a macroscopic isochiral twisting of the lamella crystal, which occurs in the form of the so-called Eshelby twist.[25] However, the underlying physics in this case can only account for a strictly monotonic increase of the band spacing with crystallization temperature and therefore is not fully applicable for the banding of PTT.

Apart from the quantitative differences in the reports on the banding behavior of PTT it is clear that our reported nonmonotonic behavior of the band spacing with crystallization temperature is very unusual and has never been observed or predicted to our knowledge. The nature of the "critical" temperature T_{CR} will be explored further using microfocus X-ray scattering data.

Spherulite Microstructure Formed at Different Crystallization Temperatures. The averaged 2D X-ray diffraction patterns acquired on banded spherulites of PTT formed at three crystallization temperatures chosen within temperature windows B_I and B_{II} (cf. Figure 2) are displayed in Figure 3. It is noteworthy that the patterns are averaged over the full radial scans across the spherulites. The central regions of the spherulites were excluded from the integration due to a strong disorientation of the crystals close to the nucleation center of the spherulite. The meridian of the patterns (vertical direction) corresponds to the crystal growth direction and thus to the crystallographic *a*-axis. The azimuthal spread of the diffraction peaks stays relatively small at all chosen crystallization temperatures.

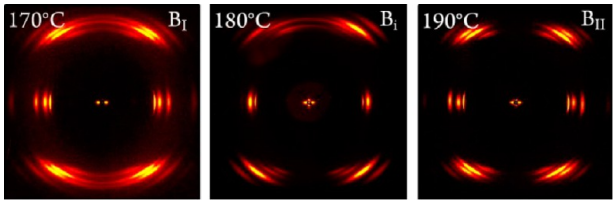

Figure 3. Averaged 2D X-ray diffraction patterns acquired on banded spherulites of PTT formed at the indicated crystallization temperatures. The radial direction of the spherulite is vertical.

The figure shows that varying the crystallization temperature from region B_I to B_{II} through the singularity point does not bring about any significant change in the local orientation of the PTT crystals. Therefore, the reason for such a strong variation of the band spacing should not be sought for in the local crystal orientation but is probably related to something else.

Inversion of the Lamellar Helicoid Chirality. To clarify the nature of the singularity point T_{CR}, a detailed analysis of the submicron X-ray diffraction patterns was performed. Integrated 1D diffractograms corresponding to a spherulite crystallized from the melt at 190 °C are given in Figure 4.

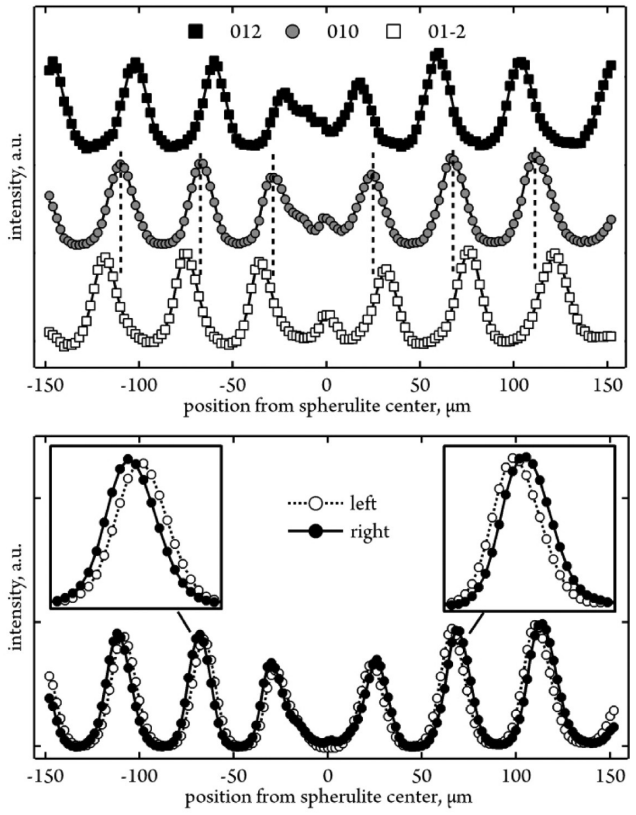

Figure 4. 1D-reduced X-ray patterns recorded during radial microfocus scans across a PTT spherulite melt-crystallized at 190 °C. In the top panel, the diffracted intensity of 012, 010, and 01−2 reflections is plotted as a function of distance from the spherulite center. The bottom panel gives the intensity of the two counterparts of the 010 peak as a function of the radial distance. The insets provide a closer view of the indicated intensity maxima.

The diffracted intensity is plotted as a function of the distance from the spherulite center. The order of appearance of the peaks as a function of the radial distance (cf. Figure 4, top panel) was found to be independent of the scanning angle, i.e., 012 → 010 → 01−2. The intensity and azimuthal position of the equatorial 010 reflection as a function of the radial distance from center allow the determination of the handedness of the lamellar helicoids using the Ewald sphere construction.[9,10,26]

It can be seen that for the shown spherulite the handedness of the lamellar helicoids is different in the spherulite sectors located on opposite sides of the spherulite center. Thus, the lamellar handedness is inverted when passing through the spherulite center. This is equivalent to the growth axis polarity changing its sign at the spherulite center. It is noteworthy that the 010 reflection stays strictly equatorial all along the radial nanofocus scan (not shown here), indicating that the direction of the *a*-axis is invariant in space. This unambiguously demonstrates that the shape of the lamella is not helical but most likely approaches the classical helicoid, as was previously found for the lamellar crystals formed at 170 °C.[10]

To identify the correlation of the growth axis polarity and lamella twist sense, a more detailed analysis of the 1D diffractograms has been carried out. The normalized intensities of selected equatorial WAXS reflections as well as the SAXS peak are given in Figure 5 as a function of the radial distance. The observed periodicity of the diffraction intensity (cf. Figure 4, top, and Figure 5) shows that the lamellar twist is regular.

dx.doi.org/10.1021/ma501733n | Macromolecules 2014, 47, 8295−8304

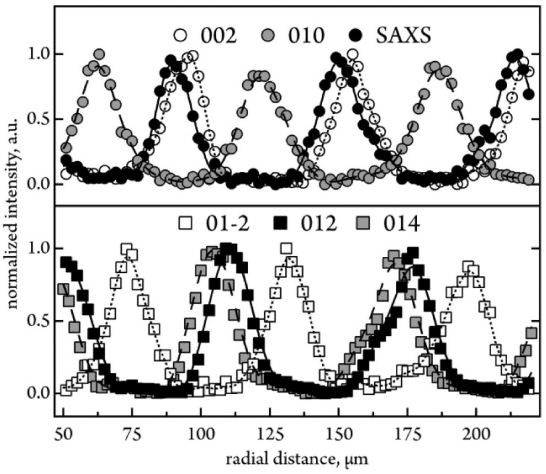

Figure 5. Normalized intensities of the strongest equatorial WAXS reflections and SAXS peak as a function of radial distance from the spherulite center.

The power spectral density function (not shown here) calculated from these curves reveals a characteristic spacing of 62.0 μm, which is in good agreement with the band spacing evaluated from the optical micrographs (cf. Figure 1).

The phase shifts of the different diffraction peaks with regard to the 010 reflection are virtually identical to the crystallographic angles calculated for the PTT reciprocal unit cell (cf. Figure 6). Thus, the lamellar twist is not only regular but also uniform. This conclusion is similar to the one drawn for the PTT films crystallized below T_{CR}.[10]

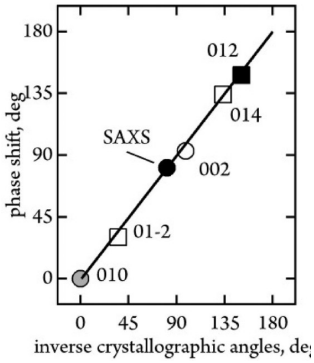

Figure 6. Phase shifts of the different equatorial reflections with respect to the 010 peak as a function of the corresponding crystallographic angles of the reciprocal unit cell.

However, the order of appearance of the main equatorial peaks, i.e., 012 → 010 → 01−2, is opposite to the situation encountered at 170 °C.[10] Therefore, the crystal rotation direction is inverted with the respect to the case reported in ref 10, as highlighted with the yellow arrow in Figure 7.

The normalized peak intensities of PTT of the main equatorial peaks of the film melt-crystallized at 180 °C are given in Figure 8 as a function of the distance from the spherulite center. At this crystallization temperature, only a slow change in the reflections intensity is visible when scanning across the entire spherulite radius. It is worth mentioning that in the acquired diffractograms (cf. Figure 3, middle) not all the reflections were visible. This can be explained by the fact that at this crystallization temperature the PTT lamellae grow as

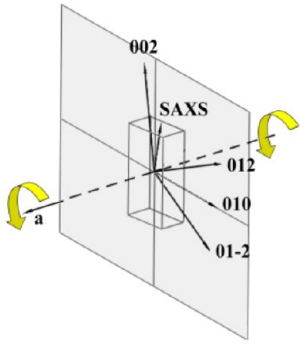

Figure 7. Model of the crystal twisting in PTT crystallized at 190 °C. The rotation axis is parallel to the crystallographic *a*-axis. The vectors corresponding to the equatorial 0*kl* reflections rotate in the *b***c**-plane. The sense of the crystal rotation is indicated by the yellow arrows.

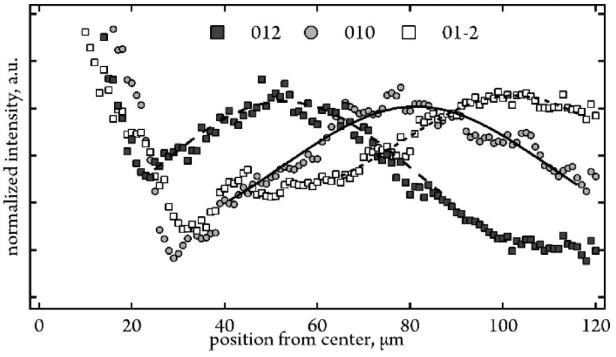

Figure 8. Normalized intensities of the strongest equatorial reflections during a radial microfocus scan across a PTT spherulite melt-crystallized at 180 °C. The integrated peak intensity is plotted as a function of distance from the spherulite center.

almost planar, single-crystalline ribbons, making it impossible to observe all diffraction peaks. Moreover, due to quasi-planarity of the lamellae, it is technically difficult to identify their handedness. Indeed, in this case not even a quarter of a full turn can be observed when scanning along the lamellae for over more than 100 μm. However, the order of appearance of the main equatorial reflections, i.e., 012 → 010 → 01−2, corresponds to the case of the B_{II} temperature region, i.e., above the T_{CR}.

The comparative models showing the correlation of the crystal rotation with the handedness of the lamellar twist for the PTT melt-crystallized at 170, 180, and 190 °C are given in Figure 9. If PTT is crystallized above ca. 179 °C, i.e., in the B_{II} temperature window, the lamella forms a right-handed helicoid when it grows in the +*a*-direction, while it forms a left-handed helicoid when growing along the −*a*-direction.

The observed correlation between the growth axis polarity (i.e., +*a* versus −*a*) and handedness of the lamellar helicoid (L versus R) can be conveniently expressed in terms of chirality parameter pairs. Thus, for temperature region B_I, the PTT structure exhibits only the lamellar helicoids characterized by (L, +*a*) and (R, −*a*) (see ref 10), while in temperature region B_{II} the structure is composed of lamellae (L, −*a*) and (R, +*a*). From this description, it is evident that when passing across the singularity point T_{CR}, one, and only one, of the two chiral parameters is inversed. It is also clear that there are no chirality parameter pairs coexist in temperature regions B_I and B_{II}.

dx.doi.org/10.1021/ma501733n | *Macromolecules* 2014, 47, 8295−8304

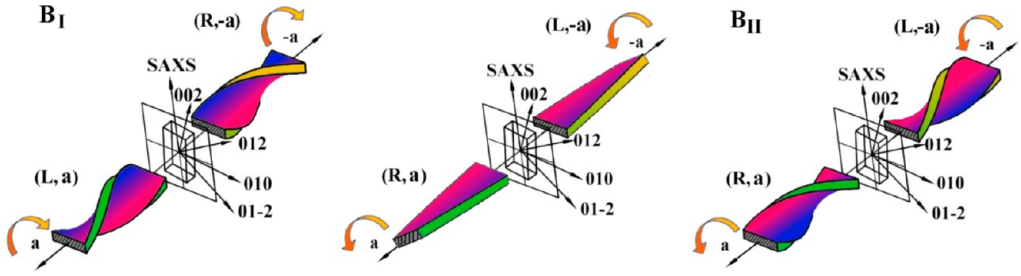

Figure 9. Sketches of the lamellar twist of the PTT melt-crystallized at 170, 180 and 190 °C (from left to right). The orange arrows indicate the rotation of the unit cell during linear growth in the *a*-directions indicated with thin black arrows.

Apart from the chirality inversion, it is important to note that, in each temperature region, only two structural states out of the theoretically possible four cases are realized. The two discussed parameters can thus be viewed as a necessary and sufficient basis of independent chirality parameters, fully expressing the structural state of the lamellar helicoids at the spatial scales addressed in this work. The physical meaning of this chirality basis will be discussed in some more detail later in the text.

Mechanics of PTT Helicoids. In the seminal model of Keith and Padden accounting for lamellar twisting,[3] the origin of the unbalanced stresses on the lamellar surface was assumed to be the tilt of the crystalline stems with respect to the lamella normal. The particular arguments used by the authors to link the chain tilt to surface stresses distribution were heavily criticized in the literature for their empirical character.[27] This is, however, in line with recent off-lattice simulations performed by Rutledge and coauthors.[28−30] The system studied in the present work provides an excellent means to check the premises of the Keith and Padden model by correlating the observed chirality of the lamellar helicoids to the observed chain tilt. In order to do so, the orientation of the unit cell was identified for the PTT films crystallized in the temperature range from 170 to 200 °C. The chain tilt was calculated using the radial offset of the equatorial reflections with regard to the main interference maximum in the SAXS region. This means that it corresponds to the inclination of the *c*-parameter with respect to the normal to the lamella in the plane perpendicular to the fast growth direction. The resulting values of the chain tilt with respect to *b**, i.e., in the plane perpendicular to the fast growth axis, are given in Figure 10 as a function of crystallization temperature.

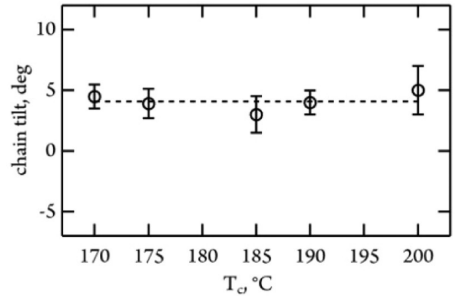

Figure 10. Chain tilt with respect to the lamella normal as a function of crystallization temperature. The graph shows no significant variation across the inversion point T_{CR} and also over a broader temperature range.

It appears that the chain tilt is virtually independent of the crystallization temperature, being equal to ca. 4.0° with a standard deviation of less than 2.0°. This means that the crystalline stems stay almost vertical in the lamellar crystal at all temperatures of crystallization. In particular, the chain tilt does not appreciably change its value across the chirality inversion point T_{CR}. Therefore, upon scrutiny, the premise of the Keith and Padden model linking the helicoid handedness with the chain tilt direction is not experimentally supported by the observations on PTT.

It is appropriate to recall that the crystalline stem conformation of PE, which Keith and Padden mainly refer to in their works, is significantly different from that of PTT. First, in the case of PE the chain forms a planar zigzag while for PTT the chain adopts a complex conformation wherein successive monomers form parts of alternating right- and left-handed helices. Thus, globally the PTT chain does not exhibit chirality, and it can be abstracted to a zigzag conformation in both the *ac* and *bc* projections. Second, the crystalline stems of PE and PTT differ remarkably in their dimensions. The *c*-parameter of the PTT unit cell is more than 7 times larger than that of PE, while the typical crystal thickness of PTT is about 4 times smaller. In a PE lamella, many tens of zigzags are present in one crystalline stem while this number is less than three for any melt-crystallized PTT. Therefore, statistically the local inclination of a single segment protruding the surface of the PE lamellae will not play any role since even a slight variation of the lamella thickness would smear out this inclination effect. By contrast, for PTT each segment of its zigzag corresponds to more than 20% of crystalline stem length. One can suggest, therefore, that instead of the overall chain-stem tilt angle, the key parameter determining the surface stresses in PTT is the angle of the crystalline stem segment protruding from the lamella surface.

To check this hypothesis, SAXS experiments on bulk samples of melt-crystallized PTT have been conducted. The obtained SAXS curves are given in Figure 11 (left column). They exhibit the main interference maximum (i.e., the long period L_B) slightly below 0.01 Å^{-1}, which shifts to smaller angles with increasing crystallization temperature. The second feature of the SAXS curves visible as a weak shoulder appears at approximately 0.02 Å^{-1}. As discussed elsewhere,[31,32] it corresponds to the form factor of the PTT crystals, which are rather monodisperse in thickness. The form factor becomes more pronounced with increasing crystallization temperatures while moving to smaller angles. The normalized 1D correlation functions (CF) calculated as a real part of the Fourier transform of the corrected scattering intensity are given in Figure 11 (middle column).

dx.doi.org/10.1021/ma501733n | *Macromolecules* 2014, 47, 8295−8304

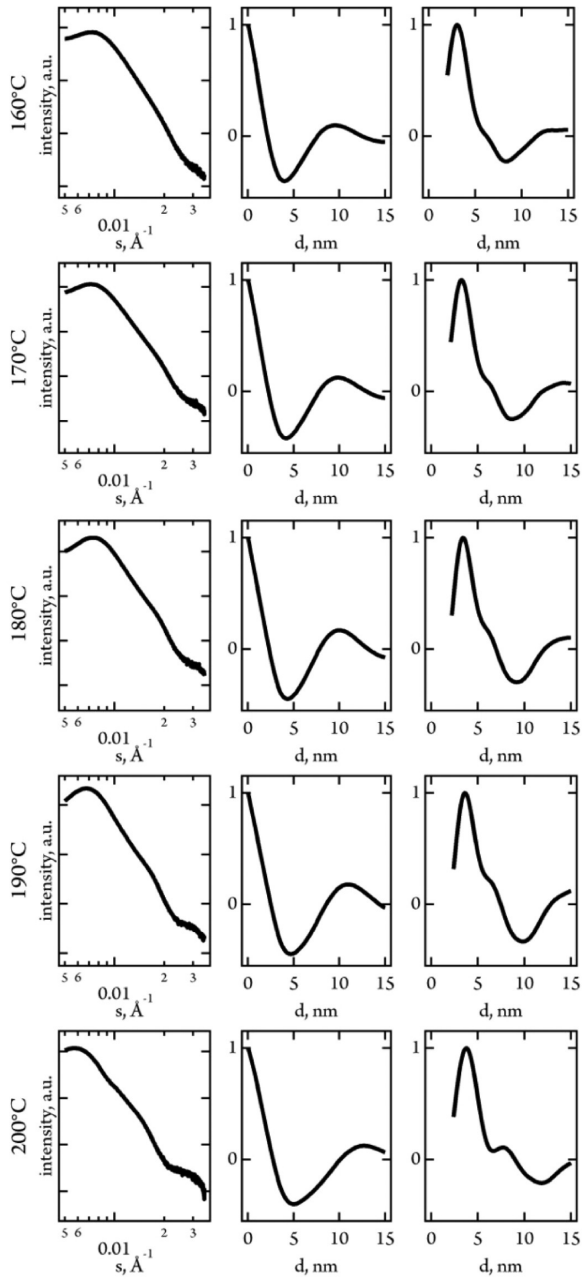

Figure 11. Experimental SAXS curves (left column) and CF and IDF functions (middle and right columns, respectively) corresponding to bulk samples of PTT isothermally melt-crystallized at the indicated temperatures.

The interface distribution functions (IDF) computed as a second derivative of the correlation functions are given in the right column of Figure 11. All IDFs exhibit either two positive maxima or one maximum and one shoulder close to the origin, which correspond to crystal thickness L_c and amorphous layer thickness L_a. The first negative maximum of the functions can be assigned to long period L_B. The crystal thicknesses values derived from the IDFs are plotted in Figure 12 as a function of crystallization temperature. They show an increment of about 20% in the temperature range from 160 to 200 °C.

At this point it is instructive to revisit the PTT band spacing dependence on crystallization temperature (cf. Figure 2). In consideration of this curve, one can ascribe a sign to the value of the band spacing, depending on the chirality of the lamellae.

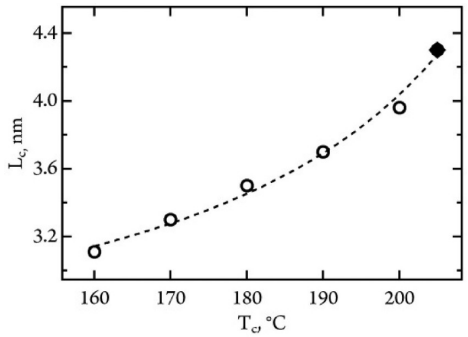

Figure 12. Lamellar thickness L_c as a function of crystallization temperature shows an increase by about 1.0 nm (or by ca. 20%) in the temperature range from 170 to 200 °C. The dashed line is a guide for the eye. The data point at 205 °C is taken from ref 32.

This is similar to what was suggested in the past for the cholesteric liquid crystals by Samulski and Samulski.[33] Using the obtained information on chirality of the lamellar helicoids, one can accordingly redraw the curve, as shown in Figure 13. In

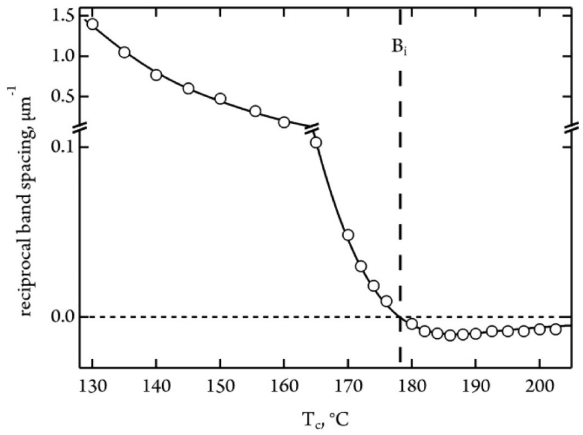

Figure 13. Reciprocal of the PTT band spacing taken with its sign reflecting the chirality of the lamellar helicoids as a function of crystallization temperature.

this case, the reciprocal band spacing in the B_{II} region is represented by negative values. This modified representation of the structural data allows an appreciation of chiral nature of the transition at T_{CR}.

Using the derived information on the crystal thickness, it is possible to check whether the experimentally derived correlation of the twisting period to the lamellar thickness is in agreement with a simple mechanical model proposed in the literature.[34] In this case, the lamellar twist period P can be described as a function of lamellar thickness L_c, elastic modulus G, and the excess surface tension due to the inherent stress γ_e according to

$$P = \frac{\pi}{6}\left(\frac{G}{\gamma_e \delta}\right) L_c^{\,2} \tag{2}$$

In eq 2, δ stands for the thickness of the surface region in which the stress is acting.

Assuming that δ is not a rapid function of crystallization temperature, one can visualize the dependence of γ_e from the lamellar thickness (cf. Figure 14). It can be seen that γ_e rapidly decays in the range of L_c values between 3.1 and 3.5 nm. Above

dx.doi.org/10.1021/ma501733n | Macromolecules 2014, 47, 8295−8304

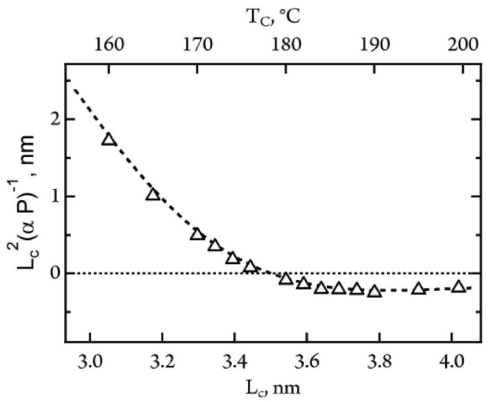

Figure 14. Reciprocal band spacing normalized by L_c^2 plotted as a function of the lamellar thickness. The α-parameter equals 1 or −1 depending on the lamellar helicoid chirality.

this range, the stresses become negative but do not evolve strongly anymore. This result shows that in modeling the twisting behavior of lamellar crystals, one cannot simply assume that the stress is a slowly changing function of the lamellar thickness as proposed for a series of aliphatic polymers by Keith and Padden.[35]

Molecular-Scale Model of Lamella Twisting. To rationalize the observed twisting behavior of the PTT crystals, one can first consider the structure of the chain, which contains rigid terephthalic units alternating with flexible propyl units, as depicted in Figure 15. The rigid parts of the chain form straight

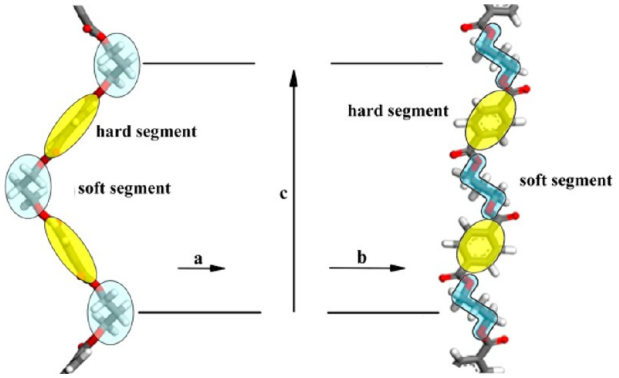

Figure 15. Schematic drawing depicting the crystalline PTT chain composed of rigid and soft sequences shown in projection on the *ac*-plane (left) and *bc*-plane (right).

segments as emphasized by the yellow ellipses. The soft segments including the semiflexible ester bonds form alternating right- and left-handed helical sequences highlighted by the light-blue clouds.

If one neglects the small overall tilt of the chain stems discussed above, the projection of one soft segment onto the *c*-axis is estimated at ca. 24% of the *c*-parameter, while the hard segment covers the rest of the half of the *c*-parameter, i.e., 26%. Taking into account that one unit cell contains two hard and two soft segments, the crystal thickness variation observed between crystallization temperature of 160 and 202.5 °C is encompassed by the length of two flexible segments. One can speculate that the segments emanating from the crystal surface into the interlamellar amorphous region must be soft because they allow the dissipation of order and density more efficiently than the rigid segments. One can notice that, when looking at the *bc*-plane (cf. Figure 15, right), i.e., along −*a*, the rigid segments are all inclined to the same side. In contrast, the middle part of the soft segment is tilted to the left, while the two parts of it which are closer to the neighboring hard segments are both tilted to the right as it is the case for the rigid segment.

A hypothetical molecular model of the PTT lamellae based on the above considerations is given in Figure 16 for

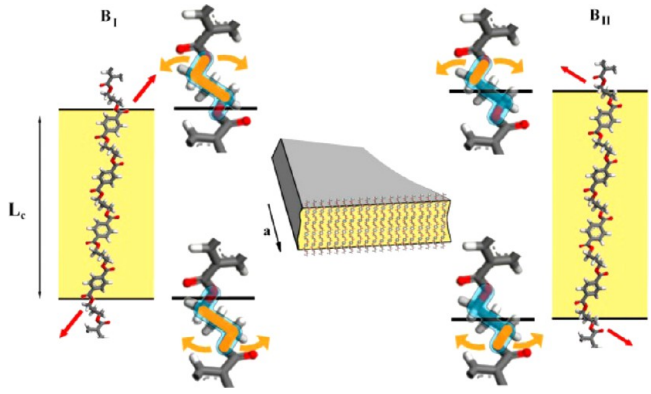

Figure 16. Schematic drawing depicting hypothetical molecular model of the PTT lamella formed at 170 and 190 °C, i.e., in B_I and B_{II} temperature regions. The direction of the bond protruding the lamellar surface is indicated with red arrows. The bonds entirely located in the amorphous phase are colored orange; their rotation freedom is indicated by the orange arrows.

crystallization temperatures within the B_I and B_{II} zones. If one considers a particular case of the PTT melt-crystallization at 170 °C, the corresponding crystal thickness is about 33 Å, i.e., ca. 1.75*c*. Assuming a symmetrical situation at both basal planes of the lamella, the soft segments will be cut by the basal planes in their first third (cf. Figure 16, left). According to our suggestion the inclination of the terminal segments should result in a left-handed twist of the lamella when growing along the positive +*a*-direction. This is indeed what is observed for PTT.[10]

For the case of PTT melt-crystallized at 190 °C (cf. Figure 16, right), the crystal thickness reaches 37 Å. The basal planes of the lamella will now intersect the soft segments in their middle, resulting in the inversion of the tilt angles of the terminal stem segments. This brings about the inversion of the lamellar twist, as it is expected.

■ CONCLUSIONS

In order to address the origin of lamella twisting in polymers, an in-depth nanofocus X-ray scattering study has been performed on banded spherulites of melt-crystallized poly(trimethylene terephthalate) (PTT). It is demonstrated that, when scanning with a microfocus X-ray beam along the spherulite radius, the diffraction peaks of the triclinic lattice of PTT show periodic intensity variations as a function of distance from the spherulite center. This indicates that the lamellar twist has a strictly uniform and regular nature. The latter observation is more compatible with models explaining the twist resulting of unbalanced surface stresses than models requiring giant screw dislocations.

Although previous literature reports demonstrated that for achiral polymers both left- and right-handed helicoids can be

dx.doi.org/10.1021/ma501733n | *Macromolecules* 2014, 47, 8295−8304

present in the same spherulite,[36] our data show that achiral polymers such as PTT are, in fact, not indifferent to the inversion of the lamellar handedness; a change in handedness is necessarily accompanied by a change in the sign of the growth vector. Therefore, our experimental observations are consonant with the first premise of the Keith and Padden (KP) model, namely, that the lamellar twist is driven by unbalanced surface stress distribution, which can be mirrored through the plane perpendicular to the growth axis and passing through the origin of the crystal, i.e., the primary nucleus. At the same time, we demonstrate that the overall chain tilt does not affect the rate and sense of twisting. This calls into question the second premise of the KP model. Instead, the local inclination of the terminal segment of the crystalline stem protruding the lamellar surface is proposed to be the key parameter controlling the surface stresses. With variation of crystal thickness as a function of crystallization temperature, the angle and direction of this terminal segment are changed, resulting in a change of the lamella twisting.

Two different temperature regions of the lamellar twisting were identified, termed B_I and B_{II}. In temperature region B_I, the band spacing increases with temperature following a second-order power law. Virtually infinite band spacing is reached at temperature T_{CR} (178.7 °C), where the spherulite exhibits essentially flat, single-crystal-like lamellae. At this point, the unbalanced surface stresses disappear, marking an inversion of the crystal rotation sense. Thus, the lamellae formed in temperature regions B_I and B_{II} differ in their chirality.

Under the assumption that the lamella surface is mainly composed of flexible segments of the PTT chain, a molecular model was constructed in which the lamellar thickness variation as a function of crystallization temperature is described in terms of the inclination angles of the soft segments protruding the crystal surface. The overall crystal thickness variation, which falls within the length of two flexible segments, allows for an explanation of the inversion of the lamellar twist sense. Within temperature regions B_I and B_{II} the crystal contains an even number of rigid segments generating a centrosymmetrical situation for the stresses on the lamellar surface.

In summary, to understand the stress distributions on the lamella surface, nanobeam X-ray diffraction experiments at the temperature of crystallization will be required. Such experiments have now become possible due to the development of a high-temperature nanocalorimetry accessory compatible with nanobeam setups.[37]

AUTHOR INFORMATION

Corresponding Authors

*E-mail: martin.rosenthal@uha.fr (M.R.).
*E-mail: dimitri.ivanov@uha.fr (D.A.I.).

Present Address

M.R.: Faculty of Fundamental Physical and Chemical Engineering, Moscow State University, GSP-1, Leninskie Gory, 119991 Moscow, Russian Federation.

Notes

The authors declare no competing financial interest.

ACKNOWLEDGMENTS

The financial support by the French Agence Nationale de la Recherche and German Research Foundation (ANR-DFG project "T2T", MO 628/13-1) is acknowledged. The authors gratefully acknowledge support by the Russian Ministry of Science and Education (project No. 11.G34.31.0055 from 19.10.2011 and project No. 14.604.21.0079). The authors are grateful to Giuseppe Portale and Wim Bras from the DUBBLE beamline (ESRF, France) as well as Sèrgio S. Funari from the A2 beamline (DESY, Germany) for fruitful discussions and excellent technical support.

REFERENCES

(1) Keith, H. D., Jr. *Polym. Sci.* **1959**, *39*, 123.
(2) Keller, A. *Polym. Sci.* **1959**, *39*, 139.
(3) Wang, Z.; Giovanni, C. A.; Hu, Z.; Zhang, J.; He, T. *Macromolecules* **2008**, *41*, 7584.
(4) Keith, H. D.; Padden, F. J. *Polymer* **1984**, *25*, 8.
(5) Keith, H. D.; Padden, F. J. *J. Appl. Phys.* **1963**, *34*, 2409.
(6) Toda, A.; Okamura, M.; Taguchi, K.; Hikosaka, M.; Kajioka, H. *Macromolecules* **2008**, *41*, 2484.
(7) Gazzano, M.; Focarete, M. L.; Riekel, C.; Scandola, M. *Biomacromolecules* **2000**, *1*, 604.
(8) Tanaka, T.; Fujita, M.; Takeuchi, A.; Suzuki, Y.; Uesugi, K.; Doi, Y.; Iwata, T. *Polymer* **2005**, *46*, 5673.
(9) Rosenthal, M.; Bar, G.; Burghammer, M.; Ivanov, D. A. *Angew. Chem., Int. Ed.* **2011**, *50*, 8881.
(10) Rosenthal, M.; Portale, G.; Burghammer, M.; Bar, G.; Samulski, E. T.; Ivanov, D. A. *Macromolecules* **2012**, *45*, 7454.
(11) Hall, I. H. *Structure of Crystalline Polymers*; Elsevier Applied Science: London, 1984; p 39.
(12) Rosenthal, M.; Anokhin, D. V.; Defaux, M.; Portale, G.; Ivanov, D. A. *J. Appl. Crystallogr.* **2011**, *44*, 805.
(13) Colombe, G.; Gree, S.; Lhost, O.; Dupire, M.; Rosenthal, M.; Ivanov, D. A. *Polymer* **2011**, *52*, 5630.
(14) Yun, J. H.; Kuboyama, K.; Ougizawa, T. *Polymer* **2006**, *47*, 1715.
(15) Chuang, W.-T.; Hong, P.-D.; Chuah, H. H. *Polymer* **2004**, *45*, 2413.
(16) Sornette, D. *Critical Phenomena in Natural Science*; Springer: New York, 2000.
(17) Auyang, S. Y. *Foundations of Complex System Theories*; Cambridge University Press: New York, 1998.
(18) Hong, P.-D.; Chuang, W.-T.; Hsu, C.-F. *Polymer* **2002**, *43*, 3335.
(19) Wu, P.-L.; Woo, E. M. *J. Polym. Sci., Part B: Polym. Phys.* **2002**, *40*, 1571.
(20) Wang, B.; Li, C. Y.; Hanzlicek, J.; Cheng, S. Z. D.; Geil, P. H.; Grebowicz, J.; Ho, R.-M. *Polymer* **2001**, *42*, 7171.
(21) Bassett, D. C.; Hodge, A. M. *Proc. R Soc. London* **1979**, *A359*, 121.
(22) Toda, A.; Keller, A. *Colloid Polym. Sci.* **1993**, *271*, 328.
(23) Toda, A.; Taguchi, K.; Kajioka, H. *Macromolecules* **2008**, *41*, 7505.
(24) Toda, A.; Arita, T.; Hikosaka, M. *Polymer* **2001**, *42*, 2223.
(25) Eshelby, J. D. *J. Appl. Phys.* **1964**, *3*, 351.
(26) Rosenthal, M.; Hernandez, J. J.; Odarchenko, Y. I.; Soccio, M.; Lotti, N.; Di Cola, E.; Burghammer, M.; Ivanov, D. A. *Macromol. Rapid Commun.* **2013**, *34*, 1815.
(27) Lotz, B.; Cheng, S. Z. D. *Polymer* **2005**, *46*, 577.
(28) Hütter, M.; In't Veld, P. J.; Rutledge, G. C. *Lecture Notes in Physics*; Reiter, G., Strobl, G., Eds.; Springer-Verlag: Berlin, 2007; Vol. *714*, pp 457−480.
(29) Rutledge, G. C.; Balijepalli, S. *J. Chem. Phys.* **1998**, *109*, 6523.
(30) Rutledge, G. C.; Lacks, D. J. *J. Phys. Chem.* **1994**, *98*, 1222.
(31) Ivanov, D. A.; Hocquet, S.; Dosiére, M.; Koch, M. H. *Eur. Phys. J. E* **2004**, *13*, 363.
(32) Ivanov, D. A.; Bar, G.; Dosiére, M.; Koch, M. H. *Macromolecules* **2008**, *41*, 9224.
(33) Samulski, T. V.; Samulski, E. T. *J. Chem. Phys.* **1977**, *66*, 2748.
(34) Okano, K. *Jpn. J. Appl. Phys.* **1953**, *24*, 176.
(35) Keith, H. D.; Padden, F. J. *Macromolecules* **1996**, *29*, 7776.
(36) Nouze, Y.; Hirano, S.; Kurita, R.; Kawasaki, N.; Ueno, S.; Iida, A.; Nishi, T.; Amemiya, Y. *Polymer* **2004**, *45*, 8299.

(37) Rosenthal, M.; Doblas, D.; Hernandez, J. J.; Odarchenko, Y. I.; Burghammer, M.; Di Cola, E.; Spitzer, D.; Antipov, A. E.; Aldoshin, L. S.; Ivanov, D. A. *J. Synchrotron Radiat.* **2014**, *21*, 223.